Chapter 4

Coordination Environment Resistant Single-Ion Magnetic Anisotropy of Seven Coordinate Ni(II) Complexes

Abstract: Ligand field mediated control of magnetic anisotropy in seven coordinate Ni(II) complexes formed by 2,6-diacetylpyridine bis(benzoyl hydrazone) and 2,6-diacetylpyridine bis(semicarbzone) have been explored. Experimental determination of D values revealed that magnetic anisotropy do not change appreciably on modifying the coordination environment of the series of mononuclear Ni(II) PBP complexes.

4.1. Introduction

Enhancement of uniaxial magnetic anisotropy is recognized as one of the most pressing challenges that need to be addressed for elevating the blocking temperature of magnetization reversal (T_b) in single molecular magnets (SMMs) [1-5]. SMM possessing large energy barrier for magnetization reversal can be assembled from even single-ion species with strong uniaxial anisotropy [6-14]. On this account, modulation of magnetic anisotropy in molecular species has become a favoured area of research during the past few years [15-16]. However, convenient approaches to enhance magnetic anisotropy have remained a grossly underdeveloped domain and control over the magnetic anisotropy is still an elusive goal.

It is widely accepted that the origin of magnetic anisotropy lies in spin-orbit coupling (SOC). SOC is operative either as in-state first order perturbation or out-of-state second order perturbation. In first row transition metal complexes, orbital degeneracy is lifted by crystal field splitting and Jahn-Teller distortion. This leads to the quenching of angular momentum and thus diminishes in-state spin-orbit interaction. Therefore, the in-state spin-orbit interaction through first order perturbation is negligible. In low coordinate complexes with symmetric and weak ligand field environment, the d-orbitals are expected to lie in a narrow energy gap. Thus, orbital angular momentum is conserved in such which results in a large SOC [17-20]. For example, in mononuclear two coordinate Fe(I) complex, large single ion anisotropy stemming from SOC results in record energy barrier for magnetization reversal [20]. However, all the known low coordinate species are extremely reactive and this limits their potential practical applications. In view of this, inducing magnetic anisotropy in transition metal complexes with high coordination geometry is an important but highly challenging task.

In case of high coordinate species with no orbital degeneracy in ground electronic state, SOC may occur through second order perturbation. Second order perturbation occurs due to the mixing of the spin-orbit states with the orbitally degenerate excited states for the orbitally non-degenerate ground state term. Thus, appropriate modulation of the excited state energy levels by modification of coordination environment should allow us to induce magnetic anisotropy in species with orbitally non-degenerate electronic ground state. In this context, several examples of seven-coordinate PBP 3d complexes are reported as potential candidates for large uniaxial anisotropy [21-31]. The planarity

of the pentadentate acylic ligand 2,6-diacetylpyridine bis(benzoyl hydrazone) (H_2L) leads to an apical structure which in turn ensures large uniaxial magnetic anisotropy. For instance, Ni(II) PBP complexes of H_2L ligand possess large uniaxial anisotropy and a large negative axial ZFS parameter (D) (Chart 4.1) [26-29, 40].

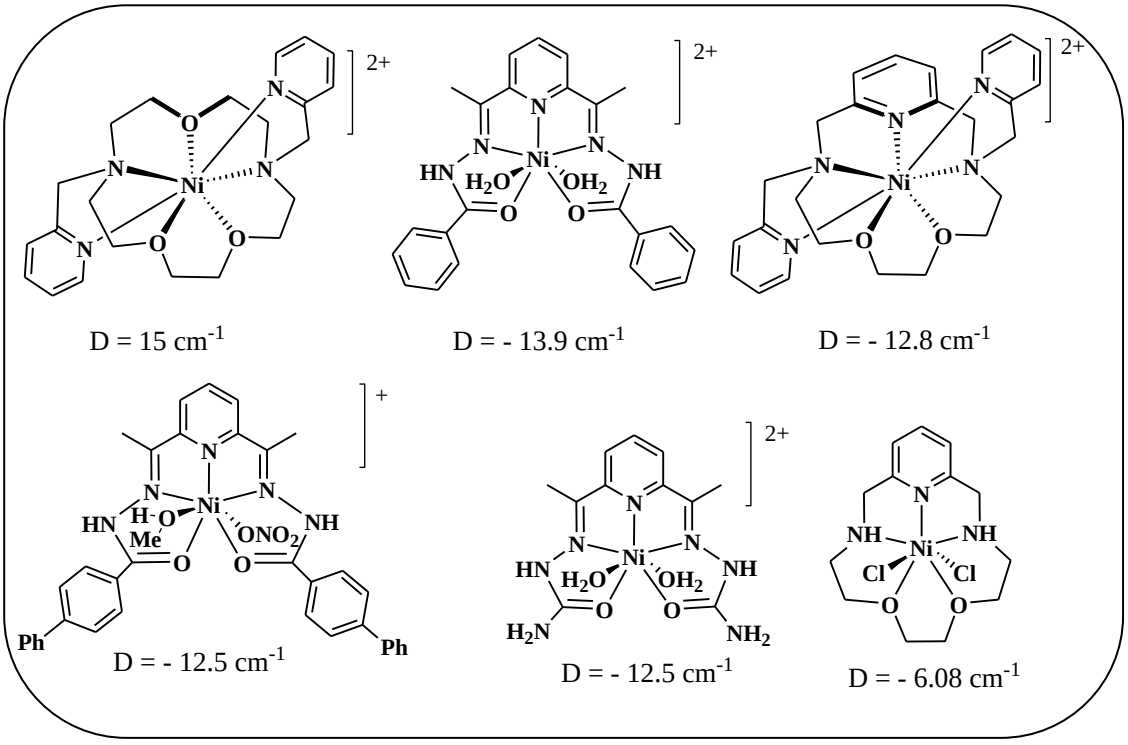

Chart 4.1. Examples of seven coordinate Ni(II) complexes for which D values have been determined

This large negative value of D in PBP Ni(II) complexes are associated with the intermingling of the orbitally non-degenerate ground electronic state with orbitally degenerate excited electronic states. Thus, mixing of the ground electronic state with excited electronic state would govern the magnitude of uniaxial magnetic anisotropy in PBP Ni(II) complexes. Herein, we investigated the possibility to control the extent of this mixing and thus tailor magnetic anisotropy by appropriate modulation of coordination environment. In this chapter, a series of PBP d^8 Ni(II) complexes of the planar pentadentate ligands, H_2L and H_2L_1 are reported (Chart 4.2). The syntheses, characterization, crystal structures and magnetic properties of four PBP Ni(II) compounds *viz*. $[Ni(H_2L)(SCN)_2].3H_2O$ (**11**), $[Ni(HL)(SCN)(H_2O)]$ (**12**), $[Ni(H_2L_1)(SCN)_2].2H_2O$ (**13**) and $[Ni(H_2L_1)(im)_2](NO_3)_2$ (**14**) have been reported.

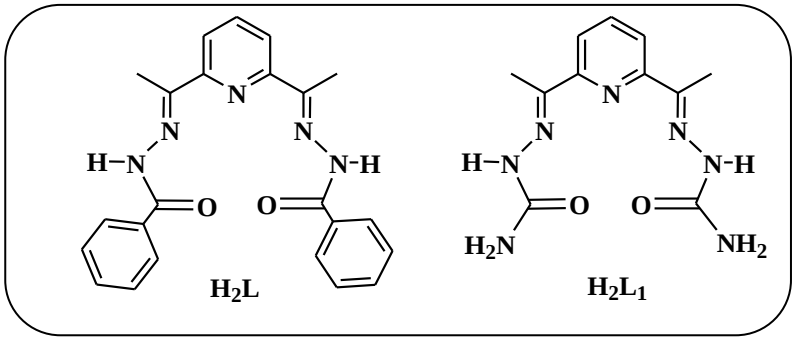

Chart 4.2. The ligands 2,6-diacetylpyridine bis(benzoyl hydrazone) (H_2L) and 2,6-diacetylpyridine bis(semicarbazone) (H_2L_1)

The D value for all the compounds were determined using magnetization measurements. Moreover, superoxide dismutase activity of these compounds has been studied spectrophotometrically using indirect nitro blue tetrazolium (NBT) assay.

4.2. Experimental Section

4.2.1. Materials and Methods

Starting materials were procured from commercial sources and used as received. Solvents were purified by conventional techniques and distilled prior to use. Elemental analyses were performed on a Perkin Elmer Model PR 2400 Series II Elemental Analyzer. Infrared spectra were recorded on a Nicolet Impact I-410 FT-IR spectrometer as KBr diluted discs and a Perkin Elmer MIR-FIR FT-IR spectrometer. The UV-visible spectra were recorded in a Shimadzu UV 2550 spectrophotometer. Melting points were recorded on a Buchi M-560 Melting Point apparatus and are reported uncorrected. Magnetic susceptibility data were collected on microcrystalline samples over a 2-300 K temperature range with an applied field of 1000 Oe using a MPMS SQUID magnetometer. Magnetization studies were performed between 0-5 T at 2 K, 5 K, 7 K and 10 K. 2, 6-diacetylpyridine bis(benzoyl hydrazone) i.e., H_2L , 2,6-diacetylpyridine bis(semicarbazone) i.e., H_2L_1, $[Ni(H_2L)(H_2O)_2](NO_3)_2$ and $[Ni(H_2L_1)(H_2O)_2](NO_3)_2$ were prepared according to the reported literature procedure [32-33].

4.2.2. Synthesis of $[Ni(H_2L)(SCN)_2].3H_2O$ (11)

To a solution of $[Ni(H_2L)(H_2O)_2](NO_3)_2$ (0.027 mmol, 0.0176 g) in methanol (20 mL), a solution of KSCN (0.056 mmol, 0.0056 g) in H_2O (10 mL) was added. The reaction mixture was stirred at room temperature for 3 hours. The reaction mixture was filtered

and the filtrate was kept undisturbed for slow evaporation at room temperature. Green block shaped crystals were observed after a week. The mother liquor was decanted and crystals were washed with minimum amount of ethanol and then dried with diethyl ether. Yield: 0.010 g (60 % based on Ni); M. p. >250°C; Elemental analysis: Found C, 47.91%; H, 3.11%; N, 15.03%. $C_{25}H_{19}N_7O_5S_2Ni$ requires C, 48.43%; H, 3.09%; N, 15.81%. IR (KBr, cm^{-1}): 3470(br), 2107(w), 2069(s), 1637(s), 1516(m), 1444(m), 1381(w), 1269(s), 1184(s),1129(w), 1012(m), 897(w), 801(m), 711(m), 554(m), 464(w).

4.2.3. Synthesis of [Ni(HL)(SCN)(H_2O)] (12)

To a solution of $[Ni(H_2L)(H_2O)_2](NO_3)_2$ (0.03 mmol, 0.0196 g) in methanol (20 mL), a solution of NaN_3 (0.013 mmol, 0.0009 g) in H_2O (5 mL) was added. The reaction mixture was stirred at room temperature for an hour. Then, a solution of KSCN (0.027 mmol, 0.0026 g) in H_2O (5 mL) was added without agitation. The reaction mixture was kept undisturbed for slow evaporation at room temperature. Red block shaped crystals were observed after 2 days. The mother liquor was decanted and crystals were washed with minimum amount of ethanol and then dried with diethyl ether. Yield: 0.012 g (75 % based on Ni); M. p. >250°C; Elemental analysis: Found C, 54.29%; H, 3.93%; N, 15.07%. $C_{24}H_{22}N_6O_3SNi$ requires C, 54.07%; H, 4.16%; N, 15.16%. IR (KBr, cm^{-1}): 3458(br), 2075(w), 1638(s), 1508(m), 1441(m), 1374(w), 1272(s), 1180(s), 1069(m), 898(w), 802(m), 710(m), 554(m), 466(w).

4.2.4. Synthesis of [Ni(H_2L_1)$(SCN)_2$].2H_2O (13)

To a solution of $[Ni(H_2L_1)(H_2O)_2](NO_3)_2$ (0.2 mmol, 0.1026 g) in methanol (20mL), an aqueous solution of KSCN (0.42 mmol, 0.0407 g) (5 mL) was added. The reaction mixture was stirred for 2 hours. The reaction mixture was then filtered and the filtrate was kept undisturbed for slow evaporation. Green block shaped crystals were observed after 10 days. The mother liquor was decanted and crystals were washed with minimum amount of ethanol and then dried with diethyl ether. Yield: 0.068 g (70 % based on Ni); M. p. >250°C; Elemental analysis: Found C, 31.92%; H, 2.99%; N, 25.87%. $C_{13}H_{15}N_9O_4S_2Ni$ requires C, 32.27%; H, 3.12%; N, 26.04%. IR (KBr, cm^{-1}): 3396(br), 2102(s), 2074(s), 1681(s), 1531(m), 1445(w), 1384(m), 1278(m), 1210(m),1094(s), 805(m), 756(m), 520(m), 462(w).

4.2.5. Synthesis of $[Ni(H_2L_1)(im)_2](NO_3)_2$ (14)

To a solution of $[Ni(H_2L_1)(H_2O)_2](NO_3)_2$ (0.1 mmol, 0.0513 g) in methanol (20 mL), a solution of imidazole (0.35 mmol, 0.0238 g) in methanol (10 mL) was added. The reaction mixture was refluxed with stirring for 2 hours. The reaction mixture was cooled to room temperature, filtered and the filtrate was kept undisturbed for slow evaporation. Green block shaped crystals were observed after 10 days. The mother liquor was decanted and crystals were washed with minimum amount of ethanol and then dried with diethyl ether. Yield: 0.046 g (89 % based on Ni); M. p. >250°C; Elemental analysis: Found C, 32.71%; H, 3.12%; N, 29.61%. $C_{17}H_{21}N_{138}Ni$ requires C, 33.62%; H, 2.99%; N, 30.00%. IR (KBr, cm^{-1}): 3191(br), 1675(s), 1621(m), 1537(s), 1384(s), 1352(w), 1196(s),1070(s), 943(w), 826(w), 801(m), 758(m), 662(m), 517(m).

4.2.6. Determination of SOD activity

The SOD activity of the Ni(II) complexes were measured by using a modified nitro blue tetrazolium (NBT) assay [34-35]. Reduction of NBT by alkaline DMSO, which acts as a source of superoxide radical ion ($O_2^{-\cdot}$) produces a blue formazan dye which can be easily detected spectrophotometrically. The % inhibition of NBT reduction was monitored against different concentration of the Mn(II) complexes. In general, 100 µL of 1.5 mM NBT was added to 1.5 mL of 0.2 M potassium phosphate buffer (pH 7.8). The tubes were kept in ice for 15 min. Then, 1.4 mL of alkaline DMSO solution was added with stirring. The absorbance was recorded at 630 nm against a sample prepared under similar condition except the addition of NaOH in DMSO. The compounds were added to the above condition before the addition of alkaline DMSO. Each experiment was performed in duplicate for different concentrations of the compounds. The concentration required to produce 50% inhibition (IC_{50}) of the reduction of NBT has been determined by linear fitting of the curve.

4.2.7. Single Crystal X-Ray Diffraction Studies

Suitable single crystals of all the compounds were obtained directly from the reaction mixtures were used for diffraction measurements. The diffraction data for the compounds were collected on a Bruker APEX-II CCD diffractometer using MoKα radiation (λ=0.71073 Å) using φ and ω scans of narrow (0.5°) frames at 90-100K. All the structures were solved by direct methods using SHELXL-97 as implemented in the

WinGX program system [36]. Anisotropic refinement was executed on all non-hydrogen atoms. The aliphatic and aromatic hydrogen atoms were placed on calculated positions but were allowed to ride on their parent atoms during subsequent cycles of refinements. Positions of N-H and O-H hydrogen atoms were located on a difference Fourier map and allowed to ride on their parent atoms during subsequent cycles of refinements.

The geometry around the Ni(II) center of mononuclear compounds **11-14** was examined using continuous shape measures analysis carried out with SHAPE program [37]. The data obtained from the analysis for compounds **11-14** are listed in Table 4.1.

Table 4.1. Shape analysis data for compounds **11-14** using SHAPE program

Complex	**HP-7**	**HPY-7**	**PBPY-7**	**COC-7**	**CTPR-7**	**JPBPY-7**	**JETPY-7**
11	33.133	23.261	1.295	7.223	5.906	2.952	22.405
12	33.394	24.703	0.763	7.570	5.788	2.486	23.053
13	33.403	23.223	0.902	8.341	6.607	2.212	23.939
14	33.840	24.231	0.340	8.249	6.481	2.512	24.159

HP-7: Heptagon (D_{7h}); HPY-7:Hexagonal pyramid (C_{6v}); PBPY-7:Pentagonal bipyramid (D_{5h}); COC-7:Capped octahedron (C_{3v}); CTPR-7: Capped trigonal prism (C_{2v}); JPBPY-7: Johnson pentagonal bipyramid J13 (D_{5h}); JETPY-7: Johnson elongated triangular pyramid J7 (C_{3v})

4.3. Results and Discussions

4.3.1. Synthesis and characterization of $[Ni(H_2L)(SCN)_2].3H_2O$ (11)

The reaction of $[Ni(H_2L)(H_2O)_2](NO_3)_2.2H_2O$ in methanol with two equivalents of KSCN resulted in the formation of green block shaped crystals of $[Ni(H_2L)(SCN)_2].3H_2O$ (**11**) in good yield (Scheme 4.1). As anticipated, the two axial sites of the precursor complex was replaced by two thiocyanate ligands leading to the formation of compound **11** with three lattice water molecules. Single crystals of compound **11** are stable at room temperature. Compound **11** was characterized by elemental analysis, FT-IR and single crystal X-ray diffraction study.

Table 4.2. Crystal data and refinement parameters of compounds **11-14**

Complex	**11**	**12**	**13**	**14**
Empirical formula	$C_{25}H_{19}N_7O_5S_2Ni$	$C_{24}H_{22}N_6O_3SNi$	$C_{13}H_{15}N_9O_4S_2Ni$	$C_{17}H_{18}N_{13}O_9Ni$
Formula weight	620.28	533.22	484.15	606.83
Temperature/K	296	296	100	296
Crystal system	Orthorhombic	Triclinic	Triclinic	Tetragonal
Space group	*P2(1)2(1)2(1)*	*P-1*	*P-1*	*I4(1)/c*
a/Å	10.330 (52)	9.009 (4)	8.758 (4)	32.159 (12)
b/Å	11.455 (3)	11.821 (5)	11.248 (5)	32.159 (12)
c/Å	23.668 (6)	11.972 (5)	12.524 (6)	10.031 (4)
α/°	90	76.66 (3)	65.78 (6)	90
β/°	90	80.41 (3)	84.96 (7)	90
γ/°	90	78.51 (3)	71.81 (6)	90
Volume/$Å^3$	2801.06 (12)	1206.14 (9)	1067.8 (9)	10374.6 (9)
Z	4	2	2	4
ρ_{calc}, g cm^{-3}	1.471	1.460	1.506	0.821
μ/mm^{-1}	0.890	0.929	1.142	1.555
Crystal size, mm^3	0.32x0.27x0.22	0.15x0.13x0.11	0.24x0.23x0.21	0.30x0.24x0.20
F(000)	1272	546	496	4976
Reflections collected	13706	6774	10441	37717
Data/parameters/restraints	6128/363/0	3839/328/0	5086/286/0	6507/373/12
Goodness-of-fit on F^2	1.057	1.063	1.050	1.375
Final R indexes [I>=2σ (I)]	R_1= 0.0489, wR_2=0.1201	R_1= 0.0609, wR_2=0.1507	R_1= 0.0606, wR_2=0.1493	R_1= 0.1120, wR_2=0.3531
Final R indexes [all data]	R_1= 0.0604, wR_2=0.1364	R_1= 0.0929, wR_2=0.1881	R_1= 0.0880, wR_2=0.1635	R_1= 0.1620 wR_2=0.3871

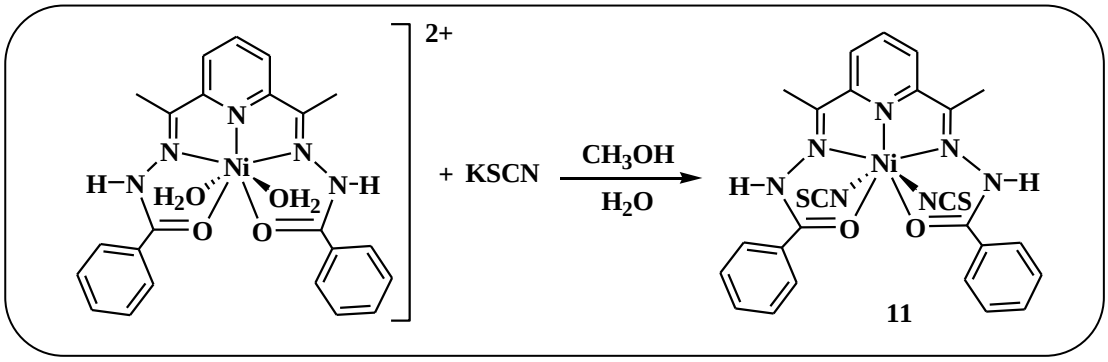

Scheme 4.1. Synthesis of compound **11**

Results obtained from the elemental analysis agree well with the proposed formulation of compound **11**. The FT-IR spectrum of compound **11** recorded as KBr disc is depicted in Figure 4.1. A broad band due to the -OH stretching of the lattice water molecules is observed at 3470 cm^{-1}. A strong absorption band is observed at 2069 cm^{-1} in the IR spectrum of compound **11**, which can be easily attributed to the stretching vibration due to the attached SCN ligand. The strong band at 1637 cm^{-1} can be assigned to the C=O stretching frequency and the band observed at 1516 cm^{-1} was due to the amide present in the bis-hydrazone ligand H_2L. The absorption peak at 1296 cm^{-1} in the spectrum is due the C=C stretching vibration of phenyl rings present in the ligand H_2L.

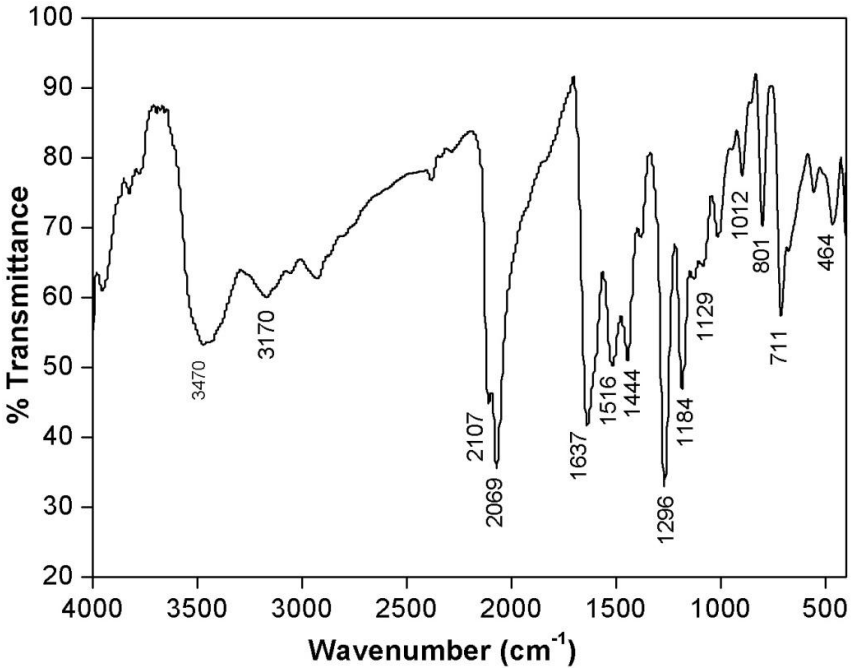

Figure 4.1. FT-IR spectrum of compound **11** as KBr diluted discs

4.3.2. Synthesis and characterization of [Ni(HL)(SCN)(H_2O)] (12)

Transition metal paramagnetic moieties bridged by small pseudohalides (N_3^-, CN^-, SCN^-, etc.) are under intense investigation due to their structural diversity leading to different magnetic exchange through them. The azide ion exhibits various bridging modes and several azido bridged aggregates with interesting magnetic properties have been reported so far [38]. Similarly, the thiocyanate ligand also exhibits different bridging modes depending on the temperature and solvent of the reaction medium [39]. So, the reaction of $[Ni(H_2L)(H_2O)_2](NO_3)_2.2H_2O$ in methanol with NaN_3 and KSCN was investigated (Scheme 4.2). However, as anticipated, the thiocyanate or azide bridged complex of the PBP Ni(II) complex was not formed. Instead, a monoanionic PBP Ni(II) complex, [Ni(HL)(SCN)(H_2O)] **(12)** with one of the axial ligand replaced by a thiocyanate liand was isolated in good yield. Red block shaped single crystals of compound **12** retain their crystallinity at room temperature.

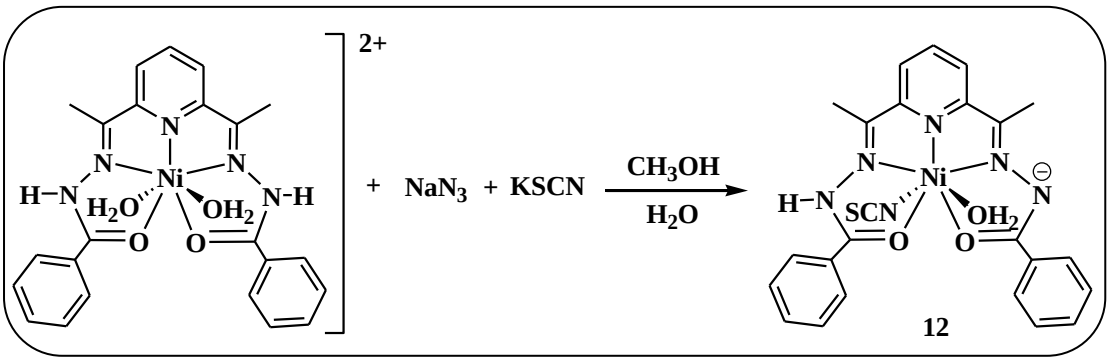

Scheme 4.2. Synthesis of compound **12**

Elemental analysis data obtained for compound **12** are in good agreement with that obtained from the proposed formulation of the compound. The FT-IR spectrum of compounds **12** is depicted in Figure 4.2. The spectrum features broad absorption band at 3458 cm^{-1} that indicates the presence of coordinated water molecule. Strong absorption band observed at 2075 cm^{-1} can be accounted for the C≡N stretching vibration of the axial thiocyanate ligands. The absorption peak due to stretching vibration of the ring from the bis-hydrazone ligand was observed at 1638 cm^{-1}. The absorption peak due the N-C=O stretching vibration present in the ligand HL are observed at 1374 cm^{-1} for the compound in the spectrum. The intense peak at 1272 cm^{-1} is due to the N-N bond stretching vibration of the ligand HL.

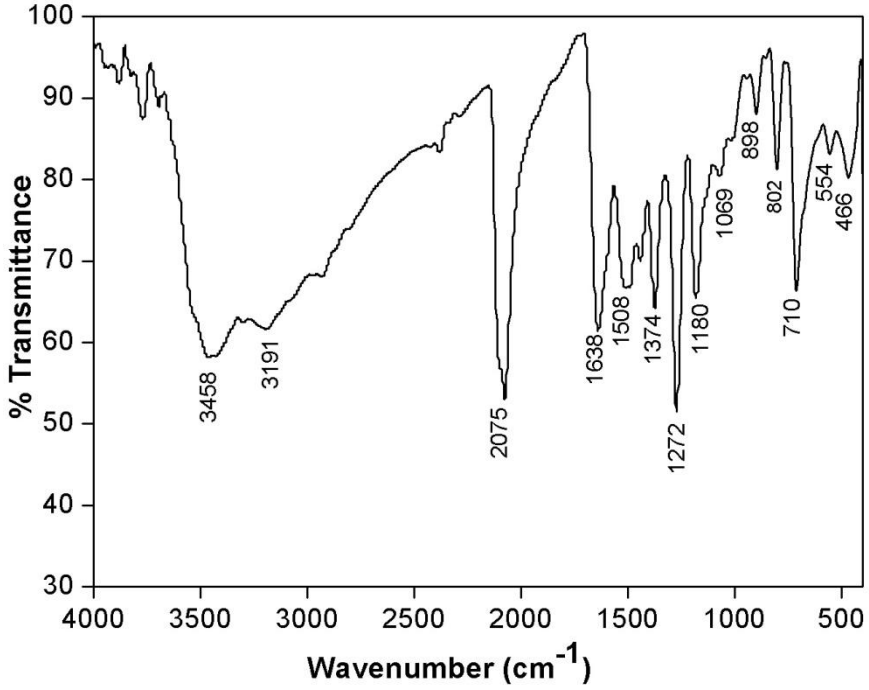

Figure 4.2. FT-IR spectrum of compound **12** as KBr diluted discs

4.3.3. Synthesis and characterization of $[Ni(H_2L_1)(SCN)_2].2H_2O$ (13)

Reaction of $[Ni(H_2L_1)(H_2O)_2](NO_3)_2$ in methanol with a slight excess of aqueous KSCN solution at room temperature yielded green block shaped crystals of $[Ni(H_2L_1)(SCN)_2].2H_2O$ (**13**) in good yield (Scheme 4.3). Single crystals of compound **13** was stable at room temperature and are further characterized with the help of elemental analysis, FT-IR and single crystal X-ray diffraction study.

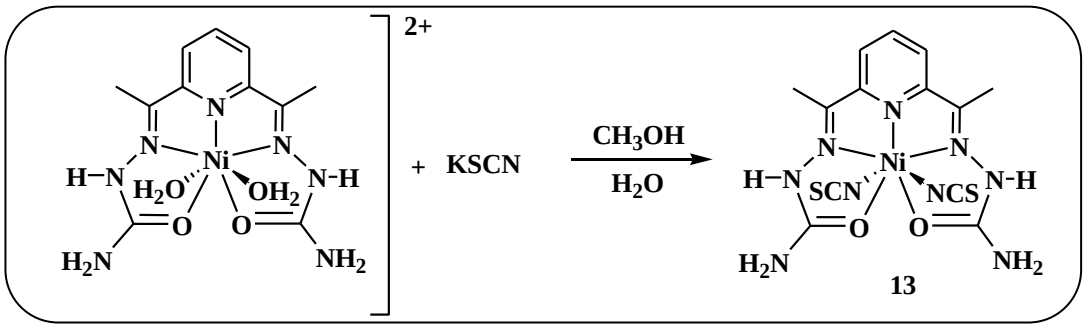

Scheme 4.3. Synthesis of compound **13**

Results obtained from the elemental analysis agree well with the proposed formulation of compound **13**. Figure 4.3 depicts the FT-IR spectrum of compound **13** recorded as KBr disc. The broad absorption peak observed at 3396 cm^{-1} can be assigned as the stretching vibrations due to the NH groups present in compound **13**. Sharp absorption peaks at 2102 and 2074 cm^{-1} have been observed due to the stretching vibrations of the

S-C≡N ligand. The absorption peak at 1681 cm^{-1} was observed due to C=N stretching vibration of the ligand. Similarly, intense peaks observed at 1537 cm^{-1} is due to coordinated C=C bond stretching vibration of the bis (semicarbazide) ligand. The N-C=O stretching vibration of the ligand H_2L_1 has been observed at 1384 cm^{-1}. The absorption band that arised due to the N-N stretching of the bis (semicarbazide) ligand, H_2L_1 was observed at 1094 cm^{-1}.

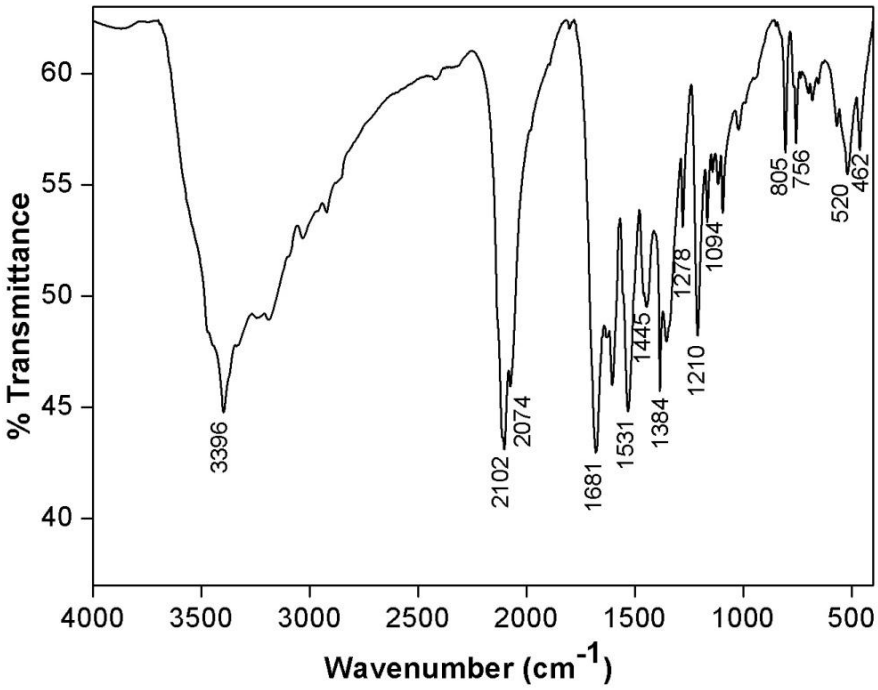

Figure 4.3. FT-IR spectrum of compound **13** as KBr diluted discs

4.3.4. Synthesis and characterization of $[Ni(H_2L_1)(im)_2].2NO_3$ (14) (im:imidazole)

Reaction of $[Ni(H_2L_1)(H_2O)_2](NO_3)_2$ in methanol with excess imidazole under refluxing condition led to the substitution of both the axial sites of the precursor Ni(II) complex by imidazole and resulted in the formation of $[Ni(H_2L_1)(im)_2].2NO_3$ (**14**) as

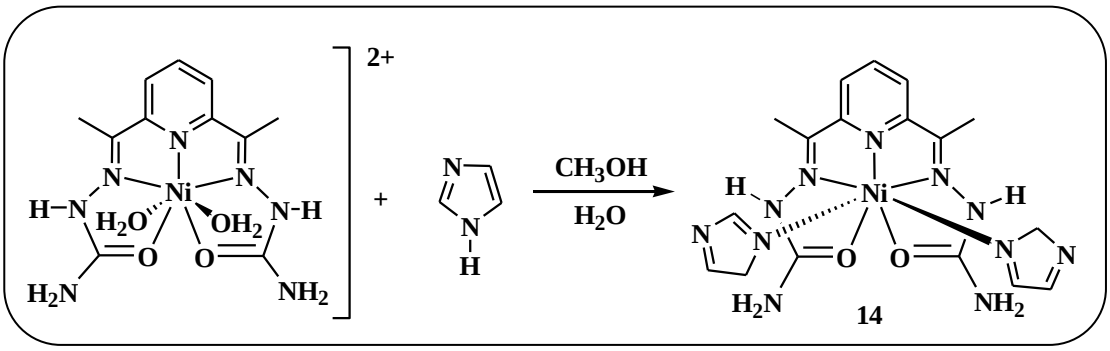

Scheme 4.4. Synthesis of compound **14**

green block shaped crystals in good yield (Scheme 4.4). Air stable single crystals of compound **14** was characterized by elemental analysis, FT-IR and single crystal X-ray diffraction study. The data obtained from elemental analysis are in good agreement with the calculated values of the proposed composition of compound **14**. Figure 4.4 depicts the FT-IR spectrum of compound **14** as KBr discs. The spectrum features broad absorption peaks at 3191 cm^{-1} which is due to the stretching vibration of the NH groups. The absorption peak due to C=N stretching vibration has been observed at 1675 cm^{-1}. The stretching vibration due to the coordinated C=C bond of the bis (semicarbazide) ligand was observed at 1537 cm^{-1}. Strong absorption peak at 1384 and 1385 cm^{-1} can be attributable to the N-C=O stretching vibration of the ligand H_2L_1. The absorption band at 1070 cm^{-1} can be assigned as the N-N stretching of the bis (semicarbazide) ligand.

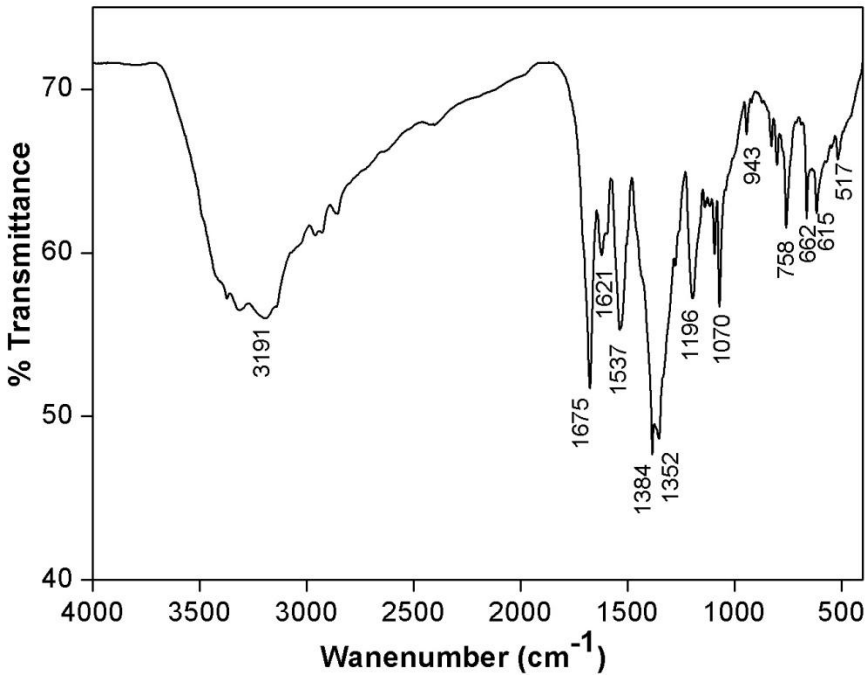

Figure 4.4. FT-IR spectrum of compound **14** as KBr diluted discs

4.3.5. Molecular structures of compounds 11-14

The molecular structures of compounds **11-14** were unambiguously established by using single crystal X-ray diffraction measurement and a representative view of the molecular structures have been depicted in Figure 4.5. Relevant crystal data along with the refinement parameters are listed in Table 4.2. All the four compounds possess PBP geometry, indicating the retention of the geometry around the Ni(II) centres of the

precursor complexes, $[Ni(H_2L)(H_2O)](NO_3)_2$ and $[Ni(H_2L_1)(H_2O)_2](NO_3)_2$. Table 4.1 depicts the shape analyses data for all the compounds. Continuous shape analyses of compounds **11-14** using the SHAPE program reveal that for all the compounds **11-14**, the mean deviations from D_{5h} PBP geometry is least among all possible seven-coordinate geometries. Selected bond lengths and bond angles of compounds **11-14** are listed in Table 4.3.

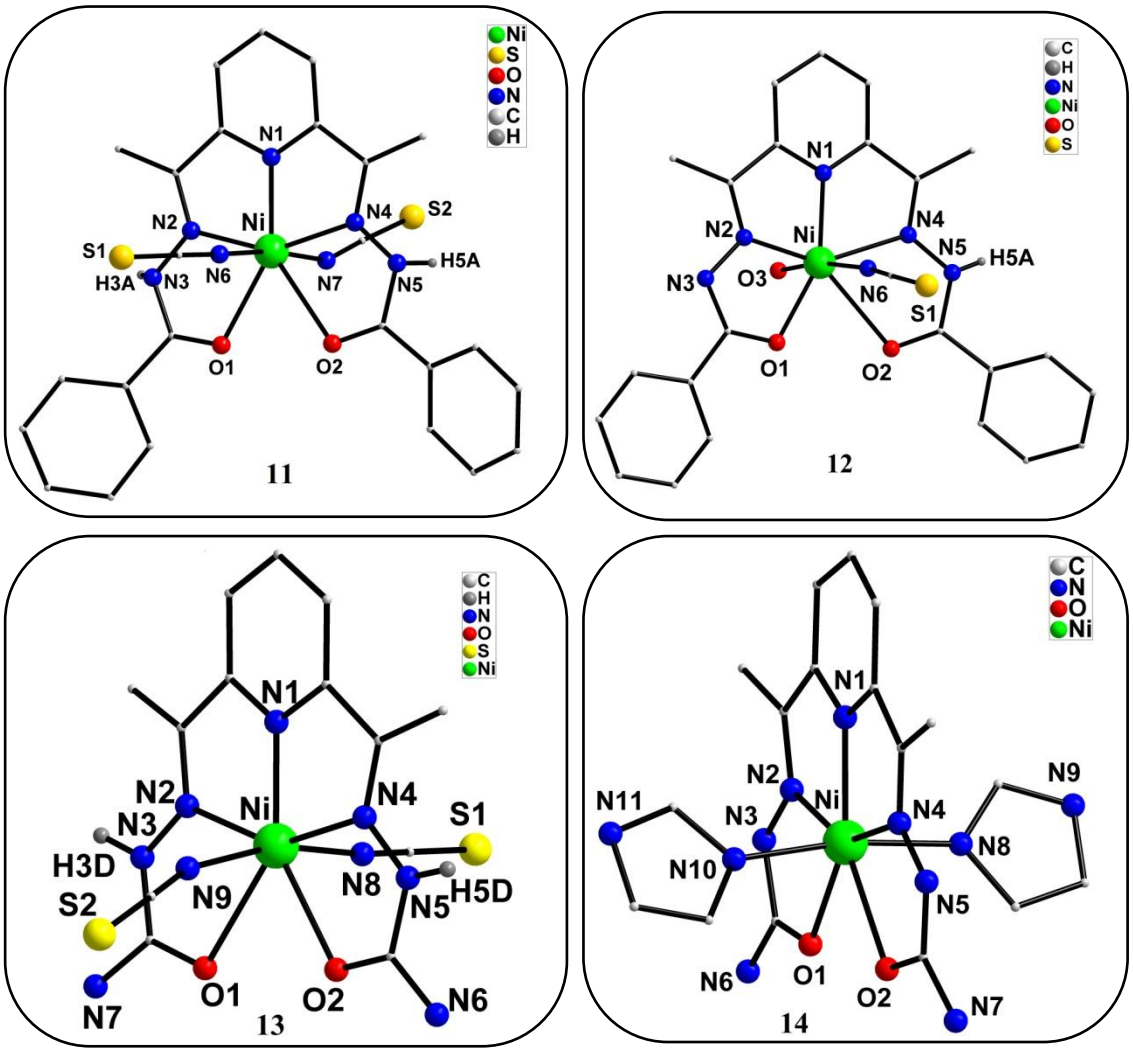

Figure 4.5. Molecular structures of compounds **11-14**. Aromatic and aliphatic hydrogen atoms are omitted for clarity. Only the N-H protons are shown wherever present

Compounds **11** and **12** were synthesized using the bis-hydrazone containing precursor complex, $[Ni(H_2L)(H_2O)](NO_3)_2$. Compound **11** crystallizes in a chiral monoclinic $P2_12_12_1$ space group with three molecules of lattice water whereas compound **12** acquires triclinic P-1 space group. The equatorial coordination sites of both the mononuclear compounds **11** and **12** are occupied by the donor atoms of bis-hydrazone

ligand, H_2L and HL respectively. The central Ni(II) atom is attached to the pyridine nitrogen atom, two imine nitrogen atoms and two oxygen atoms of the hydrazide moiety in the equatorial environment. The five donor atoms from the pentadentate ligand form an ideal planar structure for both the compounds as the sum of the chelate angles and the bite angle O(1)-Ni(1)-O(2) measures 360.29° and 360.01° in compounds **11** and **12** respectively. This confirms an ideal planar equatorial environment around the central Ni(II) atom with a N_3O_2 environment.

Table 4.3. Selected bond lengths (Å) and bond angles (◦) of compounds **11-14**

Bonds lengths	**11**	**12**	**13**	**14**
Ni-N(1)	2.015 (9)	2.068 (1)	2.021 (8)	2.087 (1)
Ni-N(2)	2.072 (9)	2.004 (1)	2.192 (7)	2.146 (1)
Ni-N(4)	2.149 (7)	2.401 (1)	2.122 (9)	2.219 (1)
Ni-O(1)	2.351 (12)	2.138 (1)	2.692 (8)	2.286 (1)
Ni-O(2)	2.643 (13)	2.824 (1)	2.393 (11)	2.468 (1)
Ni-axial(1)	2.021 (9)	2.060 (1)	1.999 (9)	2.070 (1)
Ni-axial(2)	1.993 (8)	2.002 (1)	2.003 (7)	2.051 (0)
Bond Angles	**11**	**12**	**13**	**14**
O(1)-Ni(1)-N(2)	71.17 (2)	75.51 (2)	65.15 (13)	71.29 (1)
N(2)-Ni(1)-N(1)	76.74 (2)	77.70 (2)	74.67 (14)	74.38 (1)
N(1)-Ni(1)-N(4)	74.27 (2)	69.91 (2)	75.46 (17)	73.46 (1)
N(4)-Ni(1)-O(2)	66.09 (2)	59.97 (2)	70.49 (15)	66.32 (1)
O(2)-Ni(1)-O(1)	72.02 (2)	76.92 (2)	74.16 (13)	74.54 (1)
N(1)-Ni(1)-axial(1)	94.19 (3)	91.19 (3)	95.52 (14)	94.46 (1)
N(1)-Ni(1)-axial(2)	93.40 (3)	96.89 (3)	99.02 (19)	93.64 (1)

Axial(1): SCN (**11**); H_2O (**12**); SCN (**13**); imidazole (**14**)

Axial(2): SCN (**11**); SCN (**12**); SCN (**13**); imidazole (**14**)

The average >C=N bond distances of both the compounds **11** and **12** (1.300 and 1.297 Å, respectively) are relatively longer than that that of the reported bond distances (1.189 Å) of precursor complex. The average N-N bond distances (1.342 and 1.376 Å) of both the compounds are longer as compared to the reported Ni(II) PBP precursor compound. The C-O bond distances of the hydrazone ligand in compound **11** are

shorter (1.223 Å and 1.199 Å) as compared to C-O bond distances observed in compound **12** (1.289 and 1.218 Å). One of the C-O bond distances in compound **12** is found to be longer as compared to the other C-O bond distance. Thus, it clearly indicates that in compound **11**, the pentadentate bis-hydrazone ligand is present in neutral bis-hydrazine >C=N-NH-C=O form with both the N-H protons being retained whereas in case of compound **12**, it is present in mono-anionic form with one of the N-H protons being abstracted leading to >C=N-N=C-O$^-$ form. The equatorial Ni-O bonds distances in compound **11** (2.351 and 2.643 Å) are slightly longer than the Ni-O bond distances reported for the precursor complex, $[Ni(H_2L)(H_2O)](NO_3)_2$ (2.191 and 2.346 Å). However, in compound **12** one of the equatorial Ni-O bond distance (2.138 and 2.824 Å) is significantly longer, owing to the negative charge on the oxygen atom of the deprotonated α-oxiazine arm of the ligand that strengthens one of the Ni-O bonds. The Ni-O bond is considerably elongated to avoid deposition of excess electron density on the central Ni(II) atom. Both the axial sites of compound **11** are occupied by nitrogen atoms of two thiocyanato ligands, giving rise to an overall coordination environment of N_5O_2 around the Ni(II) center. One of the Ni-N(thiocyanato) bond distances of the thiocyanate ligand attached to the central Ni(II) atom is slightly greater than the other (2.021 and 1.993 Å). In compound **12**, one of the axial sites is occupied by a thiocyanato ligand and the other by a water molecule, thus the overall coordination environment around the Ni(II) center is N_4O_3. The axial Ni-N(thiocyanato) bond distance of compound **12** measures 2.002 Å and this bond distance is comparable with that observed in case of compound **11.**

Both the mononuclear PBP Ni(II) compounds **11** and **12** show interesting hydrogen bonding architectures. The structural parameters of these hydrogen bonds are listed in Table 4.4. The nature intermolecular H-bonding pattern in compound **11** is depicted in Figure 4.8. Only the S(1) atom from one of the thiocyanate ligand forms a strong H-bond with hydrogen atoms from the imine nitrogen N(3) through the formation of N(3)-H(3A)¨S(1) bond. This H-bonding interaction leads to the a 1D chain-like structure throughout the crystal lattice in an eclipsed fashion and thereby leading to a zig-zag arrangement of the Ni^{2+} ions as depicted in Figure 4.6.

Compound **12** features interesting hydrogen bonding pattern as depicted in Figure 4.7. Only the oxygen atom O(3) of the water molecule coordinated to the axial site of the Ni(II) center participate in intermolecular hydrogen bonding with the oxygen atoms,

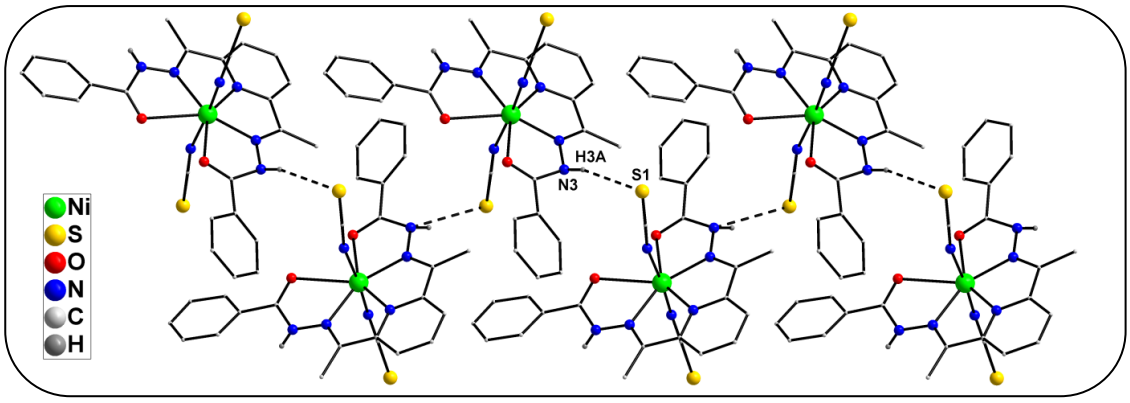

Figure 4.6. Hydrogen bonding network present in compound **11**

O(1) and O(2) of the bis hydrazone ligand of the nearby molecule leading to the formation of O(3)-H(3A)···O(1)/O(2) hydrogen bonds. This leads to the formation of a dimeric structure as depicted in Figure 4.7. The two monomeric units participating in intermolecular hydrogen bonding are situated in alternate fashion giving rise to a trans arrangement of the participating units.

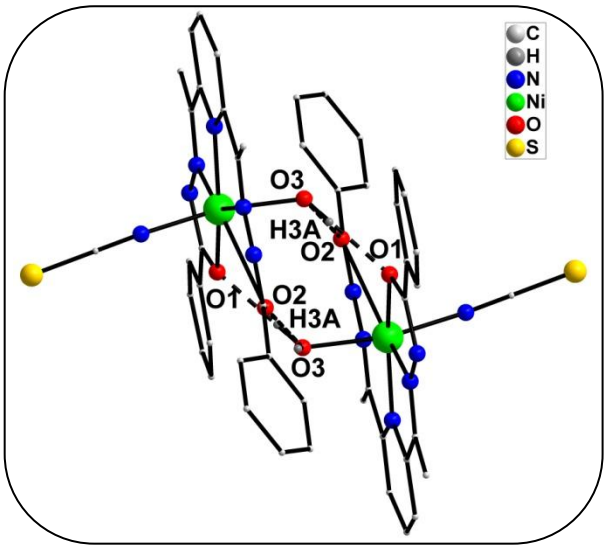

Figure 4.7. Hydrogen bonding network present in compound **12**

Compounds **13** and **14** were synthesized with the help of the semicarbazone containing ligand, H_2L_1. Compounds **13** was synthesized by following the reported procedures but its single crystal X-ray data were recollected due to unavailability of the reported data to the best of our knowledge. Compound **14** crystallizes in a tetragonal $I4_1/a$ space group with two nitrate molecules present in the lattice. The equatorial coordination sites of the mononuclear compound **13** are occupied by the donating atoms of bis-semicarbazone ligand, H_2L_1.The central Ni(II) atom is attached to the pyridine nitrogen

atom, two imine nitrogen atoms and two oxygen atoms of the semicarbazide moiety in the equatorial environment. The five donor atoms from the pentadentate ligand form an ideal planer structure. The sum of the chelate angles and the bite angle O(1)-Ni(1)-O(2) measures 359.99° in compound **14**.This validates an ideal planar equatorial environment around the central Ni(II) atom with a N_3O_2 environment.

The >C=N bond distances of the two compounds **13** and **14** are almost equal with an average distance of 1.293 and 1.308 respectively. One of the N-N bond distances for compounds **13** (1.351 and 1.372 Å) and **14** (1.359 and 1.322 Å) are slightly longer. The C-O bond distances of the semicarbazone ligand in compound **13** are equal (1.234 Å), but in compounds **14** (1.240 and 1.267 Å), one C-O bond is found to be longer as compared to the other C-O bond distance. Thus, it clearly indicates that in compound **13,** the pentadentate bis-hydrazone ligand is present in neutral bis-hydrazine >C=N-NH-C=O form with both the N-H protons being retained whereas in case of compound **14**, it is present in mono-anionic form with one of the N-H protons being abstracted leading to >C=N-N=C-O^- form. The equatorial Ni-O bonds distances in compound **14** (2.286 and 2.468 Å) are slightly shorter than the Ni-O bond distances for the compound **13** (2.393 and 2.692 Å). In compound **13**, the axial sites are occupied by nitrogen atoms of two thiocyanato ligands, giving rise to an overall N_5O_2 coordination environment around the Ni(II) center. The axial sites of compound **14** are attached with two nitrogen atoms of the imidazole molecules. Both the Ni-N(imidazole) bond distances of the imidazole moiety attached to the central Ni(II) atom are nearly equal in length (2.051 and 2.070 Å).

Both the mononuclear PBP Ni(II) compounds exhibit interesting hydrogen bonding architectures and the structural parameters of these hydrogen bonds are listed in Table 4.4. Figure 4.8 features the hydrogen bonding network of compound **13**. The two lattice water molecules participate in the formation of extensive hydrogen bonding network. The sulphur atom of the thiocyanate ligands attached to the axial sites of the compound **13** is hydrogen bonded to one of the oxygen O(102) of lattice water molecule. Moreover, the second sulphur atom of the thiocyanate ligand is involved in hydrogen bonding with the N(3) atom of the ligand H_2L through the formation of N(3)-H(3D)¨S(1) bond. This leads to the formation of a supramolecular 1D assembly in compound **13** with the successive molecules deposited in an opposite direction throughout the chain.

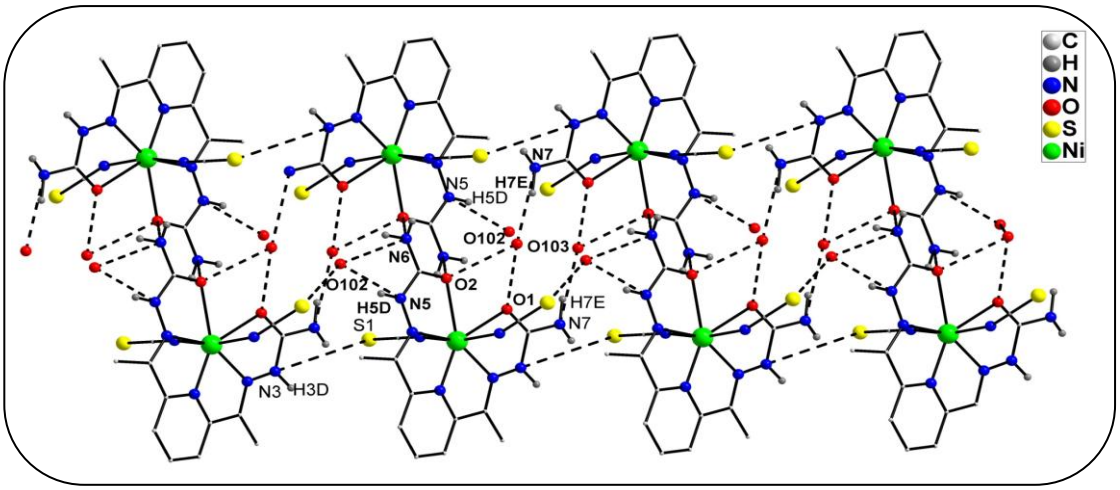

Figure 4.8.Hydrogen bonding network present in compound **13**

Table 4.4. Hydrogen bonding parameters of compounds **11**-**14**

Complex	Interactions	H···A (Å)	D···A(Å)	∠D–H···A (°)	Symmetry
11	N(3)-H(3A)···S(2)	2.66	3.487(3)	162.0	2-x, ½+y, ½-z
12	O(3)-H(3A)···O(1)	1.74	2.670(1)	157.0	1-x,1-y,-z
	O(3)-H(3A)···O(2)	2.11	2.778(1)	135.0	1-x,1-y,-z
13	N(3)-H(3D)···S(1)	2.60	3.421(16)	159.0	2-x,-y,1-z
	N(5)-H(5D) ···O(102)	2.04	2.852(14)	159.0	1+x,y,z
	N(6)-H(6D) ···O(2)	2.58	3.125(15)	125.0	1-x,1-y,1-z
	N(6)-H(6D) ···O(102)	2.22	3.106(15)	142.0	1+x, y, z
	N(7)-H(7E) ···O(103)	1.99	2.960(14)	165.0	1+x, y, z
14	N(5)-H(5A) ···O(6)	2.37	3.104(1)	131.0	1+x, y, z
	N(6)-H(6A) ···O(1)	1.97	2.904(1)	159.0	-x,-y,1-z
	N(6)-H(6A) ···O(8)	2.11	2.863(1)	131.0	1/4-y,-1/4+x,3/4+z

The hydrogen bonding network of compound **14** is shown in Figure 4.9. The oxygen atoms of the nitrate molecules present in the lattice are also hydrogen bonded to the amine nitrogen atom N(6) of the semicarbazone ligand through N(6)-H(6A)···O(8) bond. Further, the imine nitrogen atom N(5) is hydrogen bonded to one of the oxygen atom of the nitrate group present through N(5)-H(5A)···O(6) bond. The amine nitrogen atom N(6) is also hydrogen bonded to the O(1) atom of the semicarbazone ligand and

thus N(6)-H(6A)¨O(1) bond is formed. This leads to the formation of a dimeric structure throughout the crystal lattice.

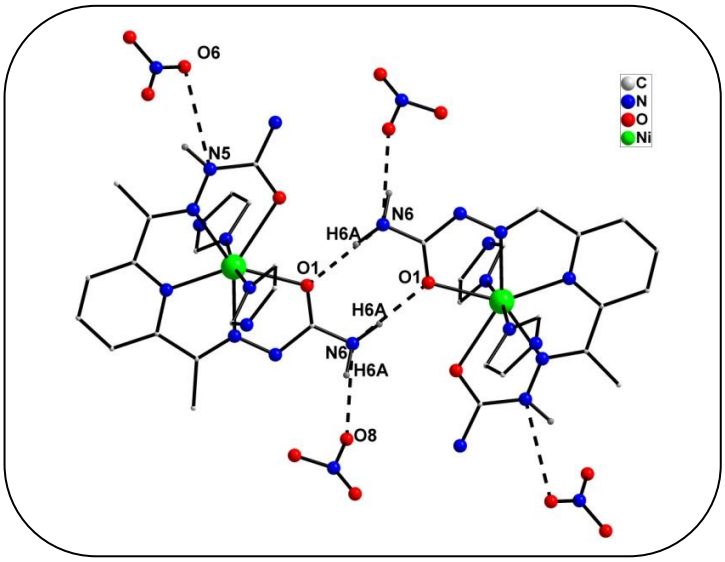

Figure 4.9.Hydrogen bonding network present in compound **14**

4.3.6. Superoxide dismutase activity

The superoxide scavenging activity of the mononuclear Ni(II) compounds **11-14** were investigated by employing a modified nitro blue tetrazolium (NBT) assay. The indirect determination of SOD activity was monitored by the reduction of NBT by superoxide generated by alkaline DMSO. As the reaction proceeds, the colour of the resulting solution changes from light yellow to blue, due to the formation of blue formazan which can be detected spectrophotometrically. Table 4.5 depicts the IC_{50} values of mononuclear PBP Ni(II) complexes **11-14** reported in this chapter. Only the mononuclear precursor complexes $[Ni(H_2L)(H_2O)_2](NO_3).2H_2O$ and $[Ni(H_2L_1)(H_2O)_2](NO_3)_2$ are catalytically active towards superoxide dismutase due to the presence of labile aqua-ligands in the axial coordination of the metal complexes which is the essential criteria for the SOD catalysis. The other synthesized mononuclear Ni(II) compounds do not show any superoxide dismutase activity. The data obtained reveals that the IC_{50} values of $[Ni(H_2L)(H_2O)_2](NO_3).2H_2O$ was found to be 5.5 µM whereas that of $[Ni(H_2L_1)(H_2O)_2](NO_3)_2$ was calculated to be 5.7 µM (Figure 4.10). The present investigation unravels that Ni-SOD can act like other SODs in the dismutation reactions, where the oxidized and reduced metal centres are Ni(III) and Ni(II) respectively. The catalytic cycle consists of two half reactions taking place via a

Ping-Pong mechanism for both native NiSOD and the metal complexes as given in the equations below.

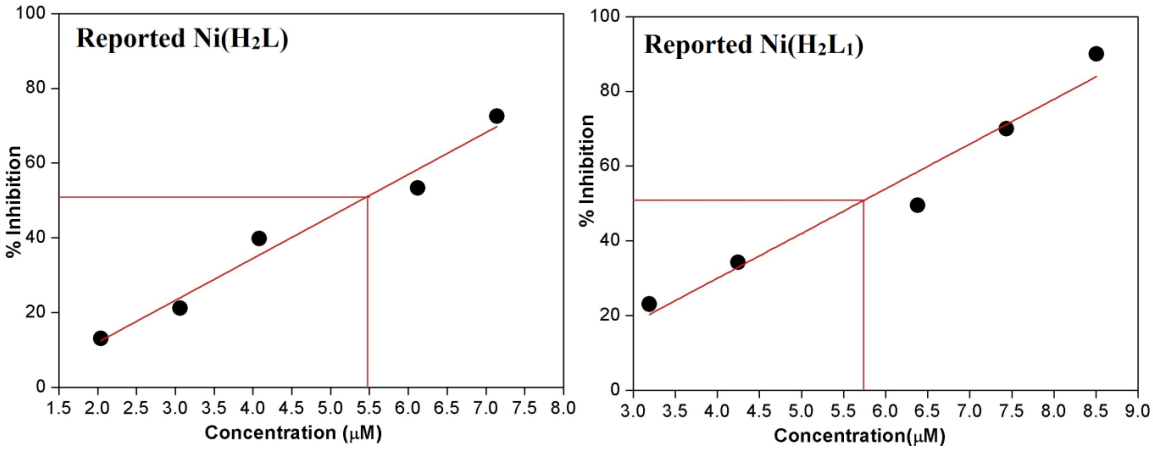

Figure 4.10. Determination of IC_{50}: Inhibition percentage as a function of the concentrations of the compounds $[Ni(H_2L)(H_2O)_2](NO_3).2H_2O$ and $[Ni(H_2L_1)(H_2O)_2].4H_2O$ respectively

$$M^{(n+1)} + SOD + O_2^{\cdot-} \longrightarrow M^{n+}\text{-}SOD + O_2$$
$$M^{n+}\text{-}SOD + O_2^{\cdot-} + 2H^+ \longrightarrow M^{(n+1)+}\text{-}SOD + H_2O_2$$

Scheme 4.5. Mechanism of SOD activity

Table 4.5. IC_{50} values of mononuclear PBP Ni(II) complexes

Sl.No.	Complexes	IC_{50} value
1.	Native NiSOD	0.05
2.	$[Ni(H_2L)(H_2O)_2](NO_3).2H_2O$	5.5
3.	$[Ni(H_2L)(SCN)_2].3H_2O$ (**11**)	Not active
4.	$[Ni(H_2L)(SCN)(H_2O)]$(**12**)	Not active
5.	$[Ni(H_2L_1)(H_2O)_2].4H_2O$	5.7
6.	$[Ni(H_2L_1)(SCN)_2]$ (**13**)	Not active
7.	$[Ni(H_2L_1)(im)_2](NO_3).H_2O$ (**14**)	Not active

H_2L: 2,6-diacetylpyridinebis(benzoyl hydrazone);

H_2L_1: 2,6-diacetylpyridinebis(semicarbazide)

4.3.7. Variable temperature magnetic studies of compounds 11-13

Magnetization studies on polycrystalline samples of compounds **11-13** were performed under a constant static field of 1000 Oe between 2-300 K. Figure 4.11 portrays the variation of $\chi_M T$ between 2-300 K for compounds **11-13** respectively. The expected $\chi_M T$ product for a magnetically isolated Ni^{2+} center considering S = 1 and g = 2.0 is 1.00 cm^3Kmol^{-1}. However at 300 K, the $\chi_M T$ product for the mononuclear Ni(II) compounds are found to be 1.29 cm^3Kmol^{-1}, 1.23 cm^3Kmol^{-1}, 1.23 cm^3Kmol^{-1} for compound **11-13** respectively, which are higher as compared to the calculated value. Deviation of $\chi_M T$ product from the expected value indicate the presence of significant orbital magnetic moment in PBP Ni(II) complexes. On lowering the temperature, $\chi_M T$ product does not change appreciably until 54 K and 60 K for compounds **11** and **12** respectively. However, on further cooling, $\chi_M T$ drops abruptly to reach a minimum of 0.76 cm^3Kmol^{-1} at 3 K for compound **11** and 0.21 cm^3Kmol^{-1} at 2 K for compound **12** respectively. For compound **13**, $\chi_M T$ product remains almost static upto to 24 K, and on further cooling, it decreases to a minimum of 0.50 cm^3Kmol^{-1} at 2 K. This deviation of

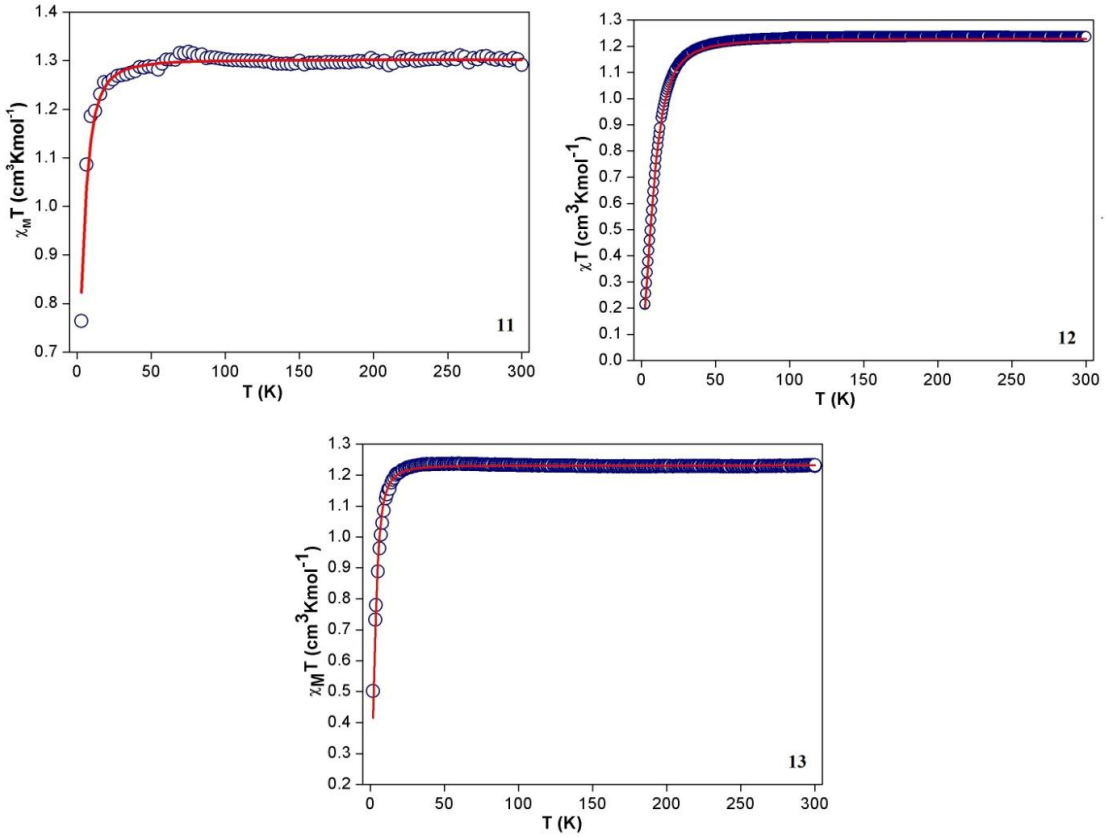

Figure 4.11. Temperature dependence of $\chi_M T$ between 2-300 K for compounds **11-13** respectively. The circles represent experimental data and the solid lines indicate the best fit obtained by using PHI program

$\chi_M T$ product from the expected value and its rapid decrease at low temperature regime indicate the presence of significant orbital magnetic moment in mononuclear PBP Ni(II) complexes. Good quality fitting of the temperature dependence of $\chi_M T$ plots of all the compounds are obtained by using PHI program and it yields g = 2.28, 2.21 and 2.21 for compounds **11-13** respectively.

Temperature dependence of $1/\chi_M$ of compounds **11-13** between 2-300 K is depicted in Figure 4.12. Curie-Weiss law is obeyed by all the compounds with a Weiss constant θ=0.662 K, 1.63 K and 0.141 K for compounds **11-13** respectively. Further, the Curie constant C is found to be 1.30 cm^3Kmol^{-1}, 1.26 cm^3Kmol^{-1} and 1.23 cm^3Kmol^{-1} for compounds **11-13** respectively. The values of C obtained experimentally for compounds **11-13** are in good agreement with the calculated C value of 1.0 cm^3Kmol^{-1} for an isolated high spin Ni(II) center with S=1 assuming g_{Ni}=2.0.The Weiss constant bears a positive sign for all the complexes, which clearly indicates that weak intermolecular ferromagnetic interactions between the spin carriers are operative in compounds **11-13**.

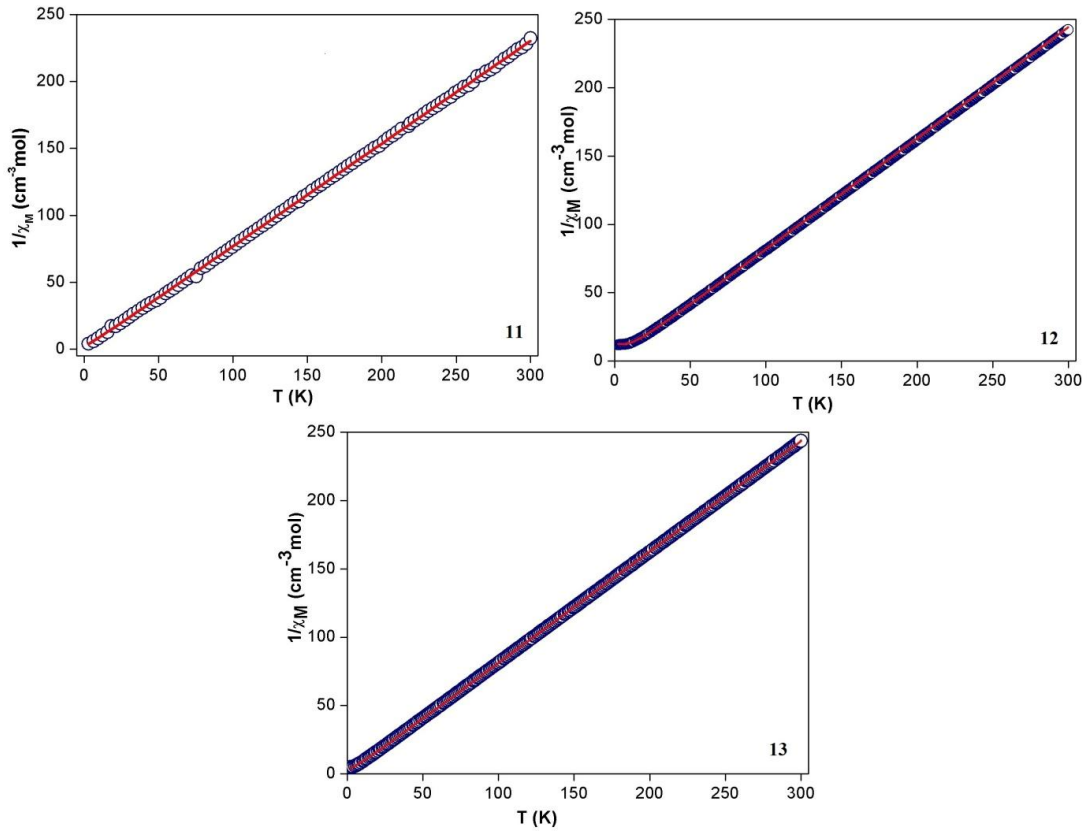

Figure 4.12. Variation of $1/\chi_M$ against temperature for compounds **11-13**. Circles represent experimental value and the solid line represents the best fit obtained by using PHI program

Isothermal field dependence of magnetization experiments were performed between 0-5 T within the temperature range of 2-10 K for compounds **11-13**. The reduced magnetization plots of compounds **11-13** have been depicted in Figure 4.13. The magnetization behaviours at 2 K, 5 K, 7 K and 10 K do not superimpose on each other in the reduced magnetization plots of all the compounds. The above observations unambiguously establish the presence of significant magnetic anisotropy in PBP mononuclear Ni(II) compounds **11-13**.

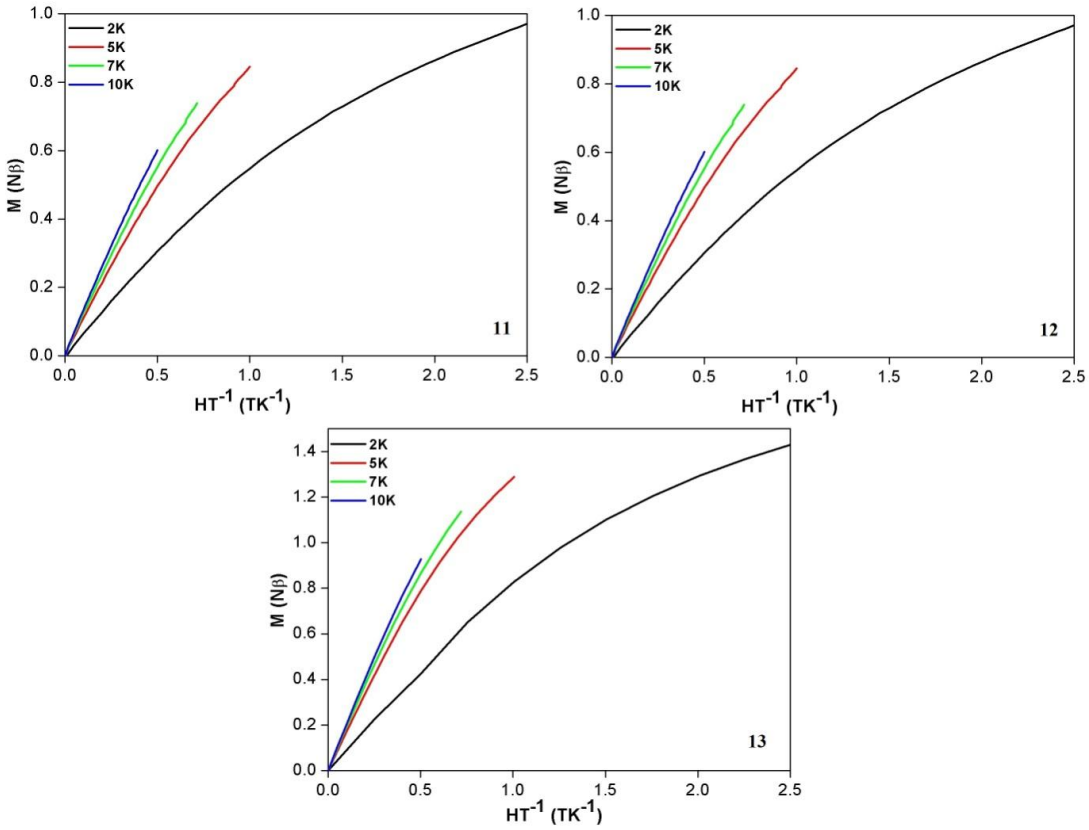

Figure 4.13. Reduced magnetization plots of compounds **11-13** respectively

Figure 4.14 depicts the field dependence of magnetization for compounds **11-13** at 2 K, 5 K, 7 K and 10 K along with the calculated value for 2 K. Although with increase of field strength, magnetization increases linearly initially, saturation magnetization M_s = 2 μB (for S = 1 and g = 2.0) was not achieved even at a field strength of 5 Tesla. The calculated magnetization behavior an isotropic S=1 system at 2 K deviated considerably from the experimental magnetization behavior for all the three compounds. This can be explained with the spin Hamiltonian equation 1:

$$\hat{H} = D[S_z^2 - S(S+1)/3] + E(S_x^2 - S_y^2) + g\beta SB \qquad (1)$$

where β, E, S and B represent Bohr magneton, rhombic ZFS parameter, spin and magnetic field vectors respectively. The best fits of the field dependant magnetization plots of compounds **11-13** obtained by using PHI program yields D = -15.66 cm^{-1}, -15.59 cm^{-1} and -16.29 cm^{-1} for compounds **11-13** respectively. The D values found for compounds **11-13** are slightly higher than the earlier reported Ni(II) complexes of D = -13.9 cm^{-1} for $[Ni(H_2L)(NO_3)(MeOH)].2H_2O$ and D = -12.5 cm^{-1} for $[Ni(H_2L)(NO_3)(OMe)](NO_3)(0.5MeOH)$ [27].

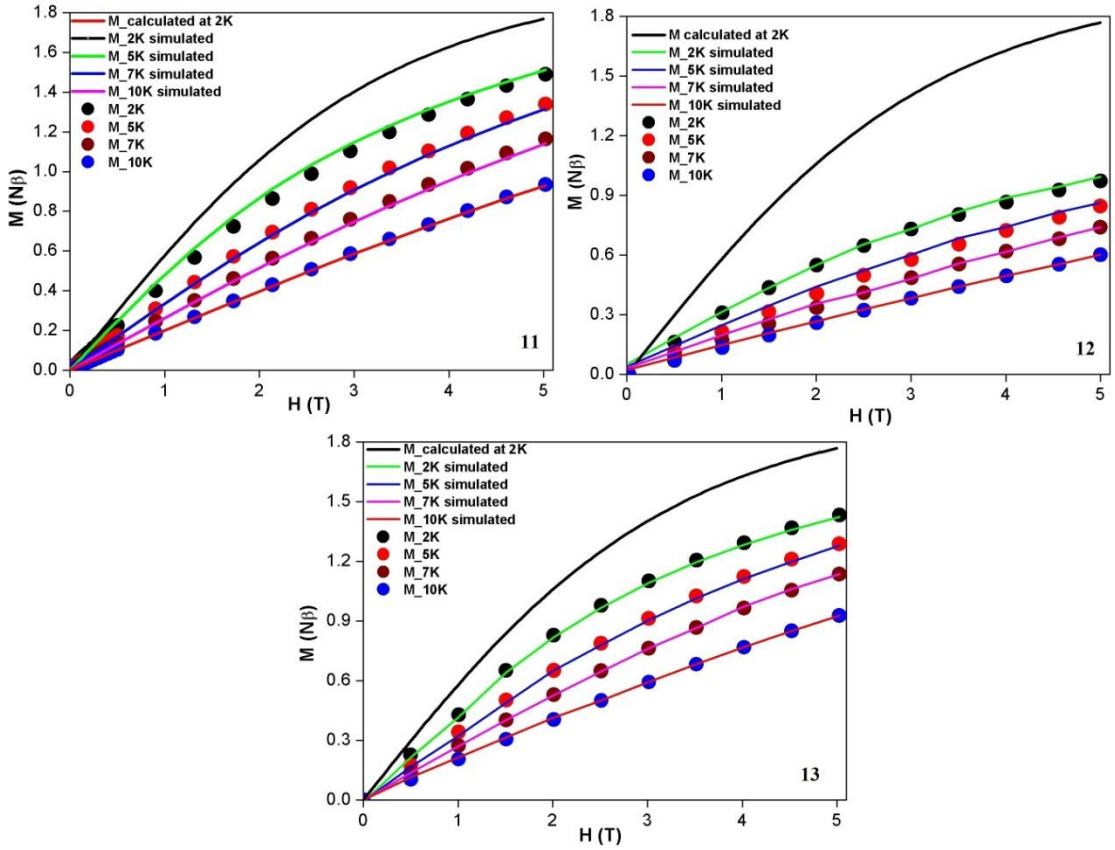

Figure 4.14. Field dependence of magnetization between 0-5 T for compounds **11-13** respectively along with the calculated magnetization behaviour for an isotropic S=3/2 system. Circles represent experimental value and the solid lines are the best fit obtained by using PHI program

The lack of any appreciable change in D values of compounds **11-13** even after altering the coordination environment significantly can be explained with the help of theoretical calculations. The mononuclear PBP Ni(II) compounds **11-13** possess a triplet ground state and involved in SOC with three triplet excited states. The electronic arrangement in the ground triplet and 1st, 2nd and 3rd excited triplet states has been depicted in Figure 4.15. The first excited state is attained by

promotion of an electron from the $d_{x^2-y^2}$ to d_{xy} orbitals. The second triplet excited state and the third triplet excited state are formed by the promotion of electrons from the d_{xz} or d_{yz} to d_{xy} and d_{z^2} orbitals respectively. On increasing the apical ligand field strength by incorporating stronger σ-donor ligands, the energy of the d-orbitals with z-components will increase. This eventually results in a decrease in energy of the second excited state and increase in energy of the third triplet excited state. Thus, the spin-orbit interaction between the triplet ground state and the second excited triplet state increases. This results in a negligible variation of the D value on tuning the ligand field geometry around the mononuclear PBP Ni(II) centre. However at the same time, the spin-orbit interaction between the ground triplet and third triplet excited energy state decreases. Due to the interplay of these two opposing effects, overall there is no variation in the D parameter of the PBP Ni(II) complexes even after the axial ligand field strength has been enhanced reasonably as compared to the reported PBP Ni(II) complexes.

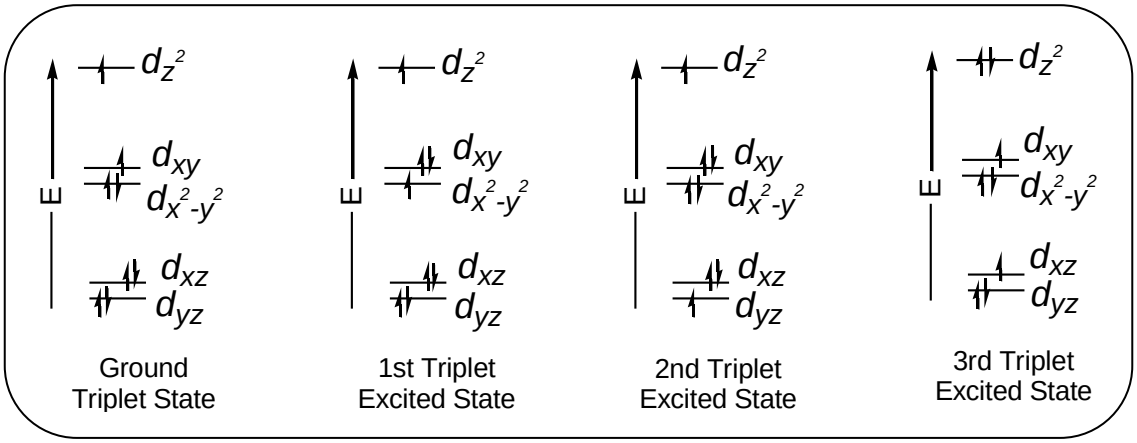

Figure 4.15. Electronic arrangement in the ground triplet and 1st, 2nd and 3rd excited triplet states

4.4. Conclusions

Four novel PBP Ni(II) compounds have been synthesized in good yield using the presynthesized compounds $[Ni(H_2L)(H_2O)_2](NO_3).2H_2O$ and $[Ni(H_2L_1)(H_2O)_2].4H_2O$ respectively. The synthesized compounds *viz*. $[Ni(H_2L)(SCN)_2].3H_2O$ (**11**), $[Ni(HL)(SCN)(H_2O)]$ (**12**), $[Ni(H_2L_1)(SCN)_2].2H_2O$ (**13**) and $[Ni(H_2L_1)(im)_2](NO_3)_2$ (**14**) have been characterized using various analytical and spectroscopic studies and a single crystal X-ray diffraction study was carried out to completely elucidate its

structure in the solid state. The magnetization studies of these mononuclear Ni(II) compounds have been performed to determine the ZFS parameters. It has been observed that contrary to the approach in mononuclear Co(II) complexes reported in the previous chapter, the ZFS parameter could not be modulated by tuning the coordination environment around the Ni(II) centre. Thus, axial ZFS parameter in PBP Ni(II) complexes are resistant to any variation even upon changing the coordination environment.

4.5. References

[1] Neese, F. and Pantazis, D.A. What is not required to make a single molecule magnet. *Faraday Discussions*, 148: 229-238, 2011.

[2] Waldmann, O. A criterion for the anisotropy barrier in single-molecule magnets. *Inorganic Chemistry*, 46(24): 10035-10037, 2007.

[3] Dey, M. and Gogoi, N. Geometry-Mediated Enhancement of Single-Ion Anisotropy: A Route to Single-Molecule Magnets with a High Blocking Temperature. *Angewandte Chemie International Edition*, 52(49): 12780-12782, 2013.

[4] Ruiz, E., Cirera, J., Cano, J., Alvarez, S., Loose, C. and Kortus, J. Can large magnetic anisotropy and high spin really coexist?. *Chemical Communications*, (1): 52-54, 2008.

[5] Bar, A.K., Pichon, C. and Sutter, J.P. Magnetic anisotropy in two- to eight-coordinated transition–metal complexes: Recent developments in molecular magnetism. *Coordination Chemistry Reviews*, 308: 346-380, 2016.

[6] Blagg, R.J., Muryn, C.A., McInnes, E.J., Tuna, F. and Winpenny, R.E. Single pyramid magnets: Dy_5 pyramids with slow magnetic relaxation to 40 K. *Angewandte Chemie International Edition*, 50(29): 6530-6533, 2011.

[7] Rinehart, J.D., Fang, M., Evans, W.J. and Long, J.R. Strong exchange and magnetic blocking in N_2^{3-}-radical-bridged lanthanide complexes. *Nature Chemistry*, 3(7): 538-542, 2011.

[8] Rinehart, J.D., Fang, M., Evans, W.J. and Long, J.R. A N_2^{3-} radical-bridged terbium complex exhibiting magnetic hysteresis at 14 K. *Journal of the American Chemical Society*, 133(36): 14236-14239, 2011.

[9] Meihaus, K.R. and Long, J.R. Magnetic blocking at 10 K and a dipolar-mediated avalanche in salts of the bis(η^8-cyclooctatetraenide) complex $[Er(COT)_2]^-$. *Journal of the American Chemical Society*, 135(47): 17952-17957, 2013.

[10] Le Roy, J.J., Ungur, L., Korobkov, I., Chibotaru, L.F. and Murugesu, M. Coupling Strategies to Enhance Single-Molecule Magnet Properties of Erbium-Cyclooctatetraenyl Complexes. *Journal of the American Chemical Society*, 136(22): 8003-8010, 2014.

[11] Ungur, L., Le Roy, J.J., Korobkov, I., Murugesu, M. and Chibotaru, L.F. Fine-tuning the Local Symmetry to Attain Record Blocking Temperature and Magnetic Remanence in a Single-Ion Magnet. *Angewandte Chemie International Edition*, 53(17): 4413-4417, 2014.

[12] Ishikawa, N., Sugita, M., Ishikawa, T., Koshihara, S.Y. and Kaizu, Y. Lanthanide double-decker complexes functioning as magnets at the single-molecular level. *Journal of the American Chemical Society*, 125(29): 8694-8695, 2003.

[13] Rinehart, J.D. and Long, J.R. Exploiting single-ion anisotropy in the design of f-element single-molecule magnets. *Chemical Science*, 2(11): 2078-2085, 2011.

[14] Jiang, S.D., Wang, B.W., Sun, H.L., Wang, Z.M. and Gao, S. An organometallic single-ion magnet. *Journal of the American Chemical Society*, 133(13): 4730-4733, 2011.

[15] Gómez-Coca, S., Aravena, D., Morales, R. and Ruiz, E. Large magnetic anisotropy in mononuclear metal complexes. *Coordination Chemistry Reviews*, 289: 379-392, 2015.

[16] Boča, R. Zero-field splitting in metal complexes. *Coordination Chemistry Reviews*, 248(9): 757-815, 2004.

[17] Zadrozny, J.M., Atanasov, M., Bryan, A.M., Lin, C.Y., Rekken, B.D., Power, P.P., Neese, F. and Long, J.R. Slow magnetization dynamics in a series of two-coordinate iron (II) complexes. *Chemical Science*, 4(1): 125-138, 2013.

[18] Zadrozny, J.M., Xiao, D.J., Long, J.R., Atanasov, M., Neese, F., Grandjean, F. and Long, G.J. Mössbauer Spectroscopy as a Probe of Magnetization

Dynamics in the Linear Iron (I) and Iron (II) Complexes $[Fe(C(SiMe_3)_3)_2]^{1-/0}$. *Inorganic Chemistry*, 52(22): 13123-13131, 2013.

[19] Poulten, R.C., Page, M.J., Algarra, A.G., Le Roy, J.J., López, I., Carter, E., Llobet, A., Macgregor, S.A., Mahon, M.F., Murphy, D.M. and Murugesu, M. Synthesis, electronic structure, and magnetism of $[Ni(6\text{-}Mes)_2]^+$: A two-coordinate nickel (I) complex stabilized by bulky N-heterocyclic carbenes. *Journal of the American Chemical Society*, 135(37): 13640-13643, 2013.

[20] Zadrozny, J.M., Xiao, D.J., Atanasov, M., Long, G.J., Grandjean, F., Neese, F. and Long, J.R. Magnetic blocking in a linear iron (I) complex. *Nature Chemistry*, 5(7): 577-581, 2013.

[21] Bartolomé, E., Alonso, P.J., Arauzo, A., Luzón, J., Bartolomé, J., Racles, C. and Turta, C. Magnetic properties of the seven-coordinated nanoporous framework material $Co(bpy)_{1.5}(NO_3)_2$ (bpy=4,4′-bipyridine). *Dalton Transactions*, 41(34): 10382-10389, 2012.

[22] Platas-Iglesias, C., Vaiana, L., Esteban-Gómez, D., Avecilla, F., Real, J.A., de Blas, A. and Rodríguez-Blas, T. Electronic structure study of seven-coordinate first-row transition metal complexes derived from 1,10-diaza-15-crown-5: A successful marriage of theory with experiment. *Inorganic Chemistry*, 44(26): 9704-9713, 2005.

[23] Schleife, F., Rodenstein, A., Kirmse, R. and Kersting, B. Seven-coordinate Mn (II) and Co (II) complexes of the pentadentate ligand 2, 6-diacetyl-4-carboxymethyl-pyridine bis (benzoylhydrazone): Synthesis, crystal structure and magnetic properties. *Inorganica Chimica Acta*, 374(1): 521-527, 2011.

[24] Drahos, B., Herchel, R. and Travnicek, Z. Structural, Magnetic, and Redox Diversity of First-Row Transition Metal Complexes of a Pyridine-Based Macrocycle: Well-Marked Trends Supported by Theoretical DFT Calculations. *Inorganic Chemistry*, 54(7): 3352-3369, 2015.

[25] Venkatakrishnan, T.S., Sahoo, S., Bréfuel, N., Duhayon, C., Paulsen, C., Barra, A.L., Ramasesha, S. and Sutter, J.P. Enhanced ion anisotropy by nonconventional coordination geometry: single-chain magnet behavior for a $[\{Fe^{II}L\}_2\{Nb^{IV}(CN)_8\}]$ helical chain compound designed with heptacoordinate Fe^{II}. *Journal of the American Chemical Society*, 132(17): 6047-6056, 2010.

[26] Ruamps, R., Batchelor, L.J., Maurice, R., Gogoi, N., Jiménez-Lozano, P., Guihéry, N., de Graaf, C., Barra, A.L., Sutter, J.P. and Mallah, T. Origin of the magnetic anisotropy in heptacoordinate Ni^{II} and Co^{II} complexes. *Chemistry–A European Journal*, 19(3): 950-956, 2013.

[27] Gogoi, N., Thlijeni, M., Duhayon, C. and Sutter, J.P. Heptacoordinated Nickel (II) as an Ising-Type Anisotropic Building Unit: Illustration with a Pentanuclear $[(NiL)_3\{W(CN)_8\}_2]$ Complex. *Inorganic Chemistry*, 52(5):2283-2285, 2013.

[28] Platas-Iglesias, C., Vaiana, L., Esteban-Gómez, D., Avecilla, F., Real, J.A., de Blas, A. and Rodríguez-Blas, T. Electronic structure study of seven-coordinate first-row transition metal complexes derived from 1, 10-diaza-15-crown-5: A successful marriage of theory with experiment. *Inorganic Chemistry*, 44(26): 9704-9713, 2005.

[29] Antal, P., Drahoš, B., Herchel, R. and Trávníček, Z. Late First-Row Transition-Metal Complexes Containing a 2-Pyridylmethyl Pendant-Armed 15-Membered Macrocyclic Ligand. Field-Induced Slow Magnetic Relaxation in a Seven-Coordinate Cobalt (II) Compound. *Inorganic Chemistry*, 55(12): 5957-5972, 2016.

[30] Huang, X.C., Zhou, C., Shao, D. and Wang, X.Y. Field-induced slow magnetic relaxation in cobalt (II) compounds with pentagonal bipyramid geometry. *Inorganic Chemistry*, 53(24): 12671-12673, 2014.

[31] Batchelor, L.J., Sangalli, M., Guillot, R., Guihéry, N., Maurice, R., Tuna, F. and Mallah, T. Pentanuclear cyanide-bridged complexes based on highly anisotropic coii seven-coordinate building blocks: synthesis, structure, and magnetic behavior. *Inorganic Chemistry*, 50(23): 12045-12052, 2011.

[32] Giordano, T.J., Palenik, G.J., Palenik, R.C. and Sullivan, D.A. Pentagonal-bipyramidal complexes. Synthesis and characterization of aqua(nitrato)[2,6-diacetylpyridine bis (benzoyl hydrazone)]cobalt(II) nitrate and diaqua[2 6-diacetylpyridine bis (benzoyl hydrazone)]nickel(II) nitrate dihydrate. *Inorganic Chemistry*, 18(9): 2445-2450, 1979.

[33] Wester, D. and Palenik, G.J. Pentagonal bipyramidal complexes of nickel (II) and copper (II). Relative importance of ligand geometry vs. crystal field effects. *Journal of the American Chemical Society*, 96(24): 7565-7566, 1974.

[34] Bhirud, R. G., and Srivastava, T. S. Synthesis, characterization and superoxide dismutase activity of some ternary copper (II) dipeptide-2, 2′-bipyridine, 1,10-phenanthroline and 2,9-dimethyl-1,10-phenanthroline complexes. *Inorganica Chimica Acta*, 179(1): 125-131, 1991.

[35] Bhirud, R. G., and Srivastava, T. S. Superoxide dismutase activity of $Cu(II)_2(aspirinate)_4$ and its adducts with nitrogen and oxygen donors. *Inorganica Chimica Acta*, 173(1): 121-125, 1990.

[36] Sheldrick, G. M. A short history of SHELX. *Acta Crystallographica Section A: Foundations of Crystallography*, 64(1): 112-122, 2008.

[37] Llunell, M., Casanova, D., Cirera, J., Bofill, J. M., Alemany, P., Alvarez, S., Pinsky, M. and Avnir, D. *SHAPE: Continuous shape measures of polygonal and polyhedral molecular fragments*; University of Barcelona: Barcelona, 2005.

[38] Ko, H.H., Lim, J.H., Kim, H.C. and Hong, C.S. Coexistence of spin canting and metamagnetism in a one-dimensional Mn (III) complex bridged by a single end-to-end azide. *Inorganic Chemistry*, 45(22): 8847-8849, 2006.

[39] Sailaja, S., Reddy, K.R., Rajasekharan, M.V., Hureau, C., Riviere, E., Cano, J. and Girerd, J.J. Synthesis, Structure, and Magnetic Properties of $[Mn^{III}(salpn)\ NCS]\ n$, a Helical Polymer, and the Dimer $[Mn^{III}(salpn)NCS]_2$. Weak Ferromagnetism in $[Mn^{III}(salpn)NCS]_n$ Related to the Strong Magnetic Anisotropy in Jahn-Teller Mn(III)(salpnH_2=N,N'-Bis(salicylidene)-1,3-diaminopropane). *Inorganic Chemistry*, 42(1): 180-186, 2003.

[40] Bar, A.K., Gogoi, N., Pichon, C., Goli, V.M.L., Thlijeni, M., Duhayon, C., Suaud, N., Guihéry, N., Barra, A.L., Ramasesha, S. and Sutter, J.P. Pentagonal Bipyramid Fe^{II} Complexes: Robust Ising-Spin Units towards Heteropolynuclear Nanomagnets. *Chemistry-A European Journal*, 23(18): 4380-4396, 2017.